Key Points:
- Largest landslides on continental slopes with low gradients and slow sediment accumulation
- Difficult to generate high excess pore pressure when sedimentation rate is low
- Sediment compressibility is a major factor for continental slope stability

Correspondence to:
M. Urlaub,
murlaub@geomar.de

What causes large submarine landslides on low gradient (<2°) continental slopes with slow (∼ 0.15 m/kyr) sediment accumulation?

Morelia Urlaub[1,2], Peter J. Talling[1], Antonis Zervos[3], and Douglas Masson[1]

[1]National Oceanography Centre, Waterfront Campus, European Way, Southampton, UK, [2]GEOMAR Helmholtz Centre for Ocean Research Kiel, Kiel, Germany, [3]Engineering and the Environment, University of Southampton, Southampton, UK

Abstract Submarine landslides can cause damaging tsunamis, the height of which scales up with the volume of the displaced mass. The largest underwater landslides are far bigger than any landslides on land, and these submarine megaslides tend to occur on open continental slopes with remarkably low gradients of less than 2°. For geohazard assessments it is essential to understand what preconditions and triggers slope failure on such low gradients. Previous work has suggested that generation of high excess pore pressure due to rapid sediment deposition plays a key role in such failures. However, submarine slope failure also occurs where sedimentation rates are low (<0.15 m/kyr), such as off northwest Africa. We use a fully coupled stress and fluid flow finite element model to test whether such low sedimentation rates can generate sufficient excess pore pressures to cause failure of a 2° slope. The sensitivity of overpressure generation and slope stability is assessed with respect to different sedimentation rates and patterns, sediment consolidation properties, and stratigraphic layer configurations. The simulations show that, in general, it is difficult to generate significant excess pore pressure if sediment accumulation is slow and the only pressure source. However, we identify a sediment compression behavior that can lead to submarine landslides in locations worldwide. Our results imply that compressibility is an important factor for the stability of low gradient continental slopes.

1. Introduction

Submarine landslides include the largest mass flows on Earth and can be up to 2 orders of magnitude larger than landslides on land [*Hampton et al.*, 1996; *Korup et al.*, 2007]. For instance, the Storegga Slide offshore Norway has a volume of over 3000 km³ and covers an area larger than Scotland [*Haflidason et al.*, 2004]. For comparison, collapse of the Mount St. Helens volcano in 1980 involved ∼3 km³ [*Voight et al.*, 1985], while the annual global flux of sediment from rivers into the ocean is ∼11 km³ [*Milliman and Syvitski*, 1992]. Submarine landslides are thus one of the major processes for moving large amounts of sediment from the continental shelf and slope into the deep ocean and play an important role in the Earth's sedimentary budget [*Masson et al.*, 2006; *Korup et al.*, 2007]. From a societal perspective, submarine landslides are important as they have caused devastating tsunamis in the past. The Storegga Slide that occurred 8200 years ago triggered a tsunami that affected the whole Nordic and North Sea region [*Bondevik et al.*, 2005]. More recently, a smaller volume slump (5–10 km³) off Papua New Guinea triggered a tsunami that killed 2200 people in 1998 [*Tappin et al.*, 2001]. The landslides themselves can damage seafloor infrastructure, such as that used for hydrocarbon exploration. They may also generate longer runout sediment flows called turbidity currents that break offshore telecommunication cables, as occurred offshore from the Grand Banks, Canada, in 1929 [*Piper and Aksu*, 1987].

While nearly all large landslides on land occur on the steepest parts of the Earth's land surface [*Korup et al.*, 2007], submarine landslides are not restricted to areas of steep slopes. Remarkably, the largest slides occur on continental slopes with gradients of 2° or less (Figure 1a) [*Hühnerbach et al.*, 2004]. Such low gradients are almost always stable on land. The high mobility of these submarine landslides is also expressed in very long runouts of several hundreds of kilometers on even smaller slope gradients [*Hampton et al.*, 1996]. The postlandslide seafloor morphology found on open continental slopes typically shows one or several bedding-parallel glide planes indicating retrogressive translational failure mechanisms (Figure 1c) [*Hampton et al.*, 1996; *Masson et al.*, 2010]. These glide planes are separated by headwalls that are often 100–250 m high (Figure 1b).
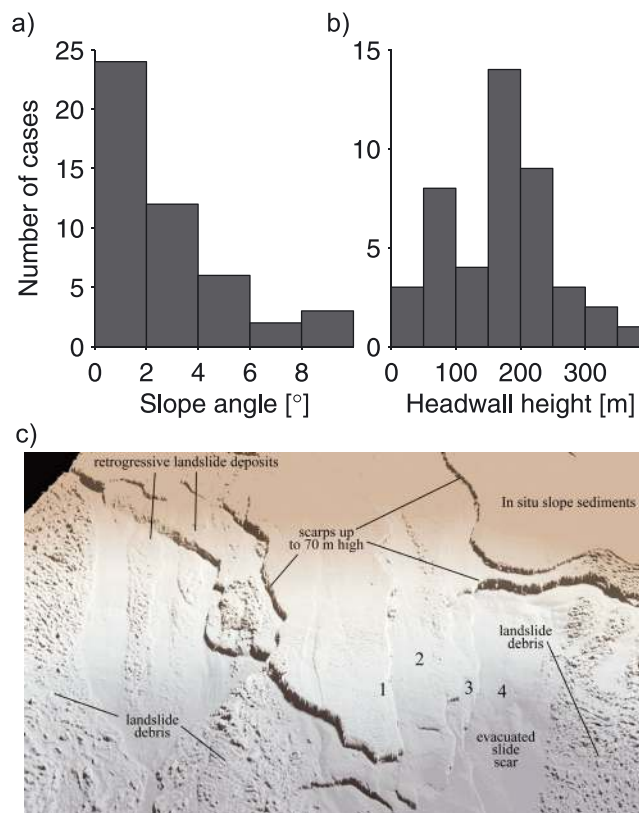
Figure 1. Typical characteristics of very large submarine landslides on open continental slopes in the Atlantic: (a) slope angles in the source areas, (b) headwall heights (compiled from *McAdoo et al.* [2000], *Hühnerbach et al.* [2004], and *Twichell et al.* [2009]), and (c) bedding-parallel glide planes in a shaded relief image of part of a large landslide on the West African continental margin [*Masson et al.*, 2010]. Water depth varies from about (top) 600 m to (bottom) 2000 m. Image is approximately 25km from left to right. Numbers indicate four distinct levels on which various sections of the landslide failed.

Interestingly, some of the largest landslides occur on passive continental margins away from major sediment input by rivers or ice streams. Examples include landslides on the northwest African continental margin [*Wynn et al.*, 2000], the southeast Australian margin [*Boyd et al.*, 2010], and the southeast Brazilian continental slope [*Kowsmann et al.*, 2002]. Estimated sediment accumulation rates for these examples are <1 m/kyr, much lower than, for example, in the Mississippi delta (>30 m/kyr [*Flemings et al.*, 2008]). This is surprising, as conventional slope stability concepts predict slopes with slow rates of sediment loading to be much more stable [*Leynaud et al.*, 2007].

1.1. Large Submarine Landslides on Low Gradients

Numerous hypotheses have been put forward to suggest mechanisms that could have the capability of triggering failure of nearly flat (<2°) slopes, including earthquakes, gas hydrate dissociation, or the presence of weak layers [*Kvalstad et al.*, 2005; *Hornbach et al.*, 2007; *Sultan et al.*, 2004; *Masson et al.*, 2010]. However, the reason(s) for large-scale failure of low-angle submarine slopes are contentious and their understanding is complicated by the lack of direct observations and in situ monitoring [*Talling et al.*, 2014]. Moreover, it is important to distinguish between factors that precondition or trigger slope failure. This lack of consensus makes risk assessment more difficult than for other geohazards.

The morphological similarity of many large landslides suggests a similar failure mechanism, and possibly also similar geotechnical and rheological properties of the failed material [*Locat and Lee*, 2002]. The failure of slopes with inclination of <2° is difficult to explain, as this is well below typical friction angles for any type of sediment. To overcome the sediment's shearing resistance and to cause failure at such low slope angles, it is expected that pore pressures greatly exceed the hydrostatic pressure. A simple infinite slope calculation using the critical state strength, ϕ'_{crit}, as strength parameter, shows that for a < 2° slope pore pressure must take up more than 94% of the lithostatic stress to destabilize sediment with a strength of $\phi'_{crit} = 30°$ (Figure 2). For slopes
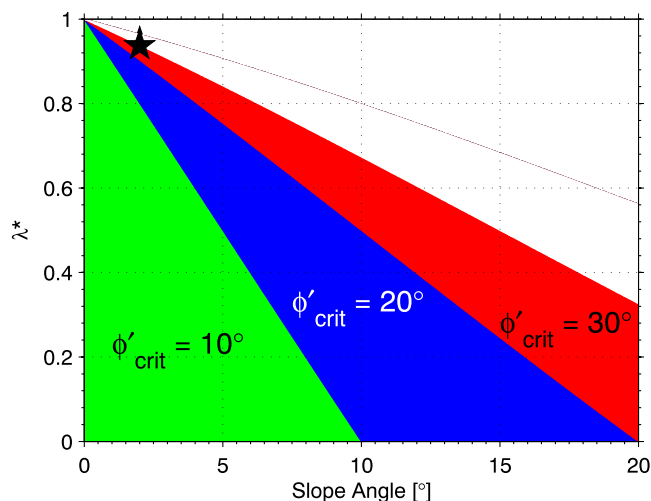
Figure 2. Slope stability as a function of slope angle and overpressure ratio, λ^* (equation (1)), according to infinite slope analysis. All combinations of slope angle and overpressure in the green/blue/red fields are stable for a sediment that has a minimum critical friction angle, ϕ'_{crit}, of 10°/20°/30°. For example, a 2° slope made of sediment with $\phi'_{crit} = 30°$ is stable unless λ^* exceeds 0.94 (black star).

of less strong material, e.g., $\phi'_{crit} = 10°$ or $\phi'_{crit} = 20°$, it still takes pore pressures higher than 80% of the lithostatic stress (Figure 2). A useful measure for the degree of overpressurization of the slope is the overpressure ratio, λ^*, which is the ratio of excess pore pressure, p_e, to vertical effective stress in hydrostatic conditions:

$$\lambda^* = \frac{p_e}{\sigma_v - p_h}.$$ (1)

Pore pressures in excess of hydrostatic have been measured by drilling at several continental margins worldwide [e.g., *Kvalstad et al.*, 2005; *Flemings et al.*, 2008]. Laboratory experiments and modeling have shown that consolidation of soft marine sediments during burial can generate excess pore pressures when certain preconditions, such as high sedimentation rates, are fulfilled [*Binh et al.*, 2009; *Stigall and Dugan*, 2010]. Modeling has shown that rapid (~30 m/kyr) and prolonged (several thousand years) sediment deposition from river discharges or ice streams can generate sufficiently high overpressure ratios to directly cause failure of nearly flat slopes or weaken the slope to an extent that a moderate earthquake can cause failure [*Stigall and Dugan*, 2010]. Slope failure may also occur as a result of focused lateral fluid flow from areas of high overburden into areas of low overburden [*Dugan and Flemings*, 2000; *Flemings et al.*, 2002].

These modeling efforts are, however, limited to open continental slopes with relatively high (> 1 m/kyr) sediment input, such as the Gulf of Mexico. It is noteworthy that some of the largest submarine landslides occurred at continental margins with much lower sedimentation rates [*Wynn et al.*, 2000; *Twichell et al.*, 2009; *Krastel et al.*, 2012]. Simple 1-D modeling predicts that the generation of excess pore pressure is small when sedimentation rates are low [*Gibson*, 1958; *Urlaub et al.*, 2012]. It is as yet to be modeled whether particular consolidation properties, slope loading patterns, or property contrasts of slope sediments favor the generation and retention of excess pore pressures even if sedimentation rates are low. In this contribution we assess for the first time how slope failure could occur in slow (< 0.15 m/kyr) sedimentation settings.

1.2. Aims and Objectives

This study focuses on open continental slopes at passive margins with headwall heights in excess of 100 m, because they host many of the largest submarine landslides. The aim of this contribution is to characterize the general behavior of a submerged 2° continental slope with low sediment accumulation. This is in contrast to previous studies whose focus was mainly on case studies [*Dugan and Flemings*, 2000, 2002; *Binh et al.*, 2009; *Hustoft et al.*, 2009; *Stigall and Dugan*, 2010]. Moreover, there is currently no study that quantifies the term "rapid" with respect to excess pore pressure generation due to rapid deposition. Such a quantification is necessary, as rapid deposition has been used to explain slope failure for a wide spectrum of sedimentation rates [*Antobreh and Krastel*, 2007; *Lee*, 2009]. It also remains unknown what rates and patterns of deposition or stratigraphy are required for focused fluid flow to take place in amounts high enough to cause failure or weaken the slope. Therefore, the key questions addressed in this contribution are as follows:

1. Can low sedimentation rates (<0.15 m/kyr) generate sufficient excess pore pressure in a 2° slope to cause its failure?
2. What are the critical factors that control excess pore pressure generation and stability of a 2° slope if low sediment accumulation is the only pressure source?
3. Under which circumstances can the identified critical factors be realistically expected?

We investigate the dependence of stability on three main factors that can control the development of overpressure: spatial as well as temporal sedimentation patterns, hydromechanical properties of deep sea sediments (compressibility, permeability, permeability anisotropy, and friction angle), and the pore fluid flow pattern caused by permeability contrasts. To explore the effect of permeability and compressibility, we use a 1-D sedimentation-consolidation approach. For settings in which two dimensions are required due to lateral flow or spatial distribution of stresses, we use 2-D finite element (FE) models.

2. Methodology

2.1. One-Dimensional Sedimentation-Consolidation Analysis

Assuming that low sediment accumulation with a rate of 0.15 m/kyr is the only pressure source, we calculate excess pore pressures using the 1-D analysis presented by *Viesca and Rice* [2012] for steady, long-time sedimentation with consolidation on a slope. We aim to identify critical values for compressibility, λ, and permeability, k, of the sediment required to generate excess pore pressures sufficiently high to cause failure of a 2° slope (Figure 2). A single material is modeled without abrupt changes in its physical or mechanical properties. Compaction occurs in the downward direction only. Void ratio, e, which relates to porosity, n, by $e = \frac{n}{1-n}$ for fully saturated soils, declines with effective pressure, p'. This decline is prescribed in the Modified Cam Clay model ($e = e_0 - \lambda \cdot \ln(p')$) with $e_0 = 3.0$ at unity (1 kPa). Permeability depends on porosity following the relationship for hemipelagic mud from *Flemings et al.* [2012] (original equation converted to give k in m/s instead of m^2 for seawater at ~15°C):

$$k_z = 10^{-15.48} \, \text{m/s} \cdot 10^{9.4 \cdot n}. \tag{2}$$

We use λ to calculate the coefficient of consolidation, c_v, according to $c_v = k \cdot E_0 \cdot \gamma_w^{-1}$. We use Young's modulus $E_0 = 3K(1 - 2\nu)$, bulk modulus $K = (1 + e) \cdot p' \cdot \lambda^{-1}$, specific weight of water $\gamma_w = 10 \, \text{kN} \cdot \text{m}^{-3}$, and Poisson ratio $\nu = 0.3$.

2.2. Two-Dimensional Finite Element Consolidation and Slope Stability Modeling

A 2-D model is used where lateral flow or spatial distribution of stresses is important. In our fully coupled fluid flow and stress analysis a porous medium is modeled by attaching the finite element (FE) mesh to the solid phase. The fluid flow is governed by Darcy's law considering a single incompressible pore fluid (seawater). The mechanical part of the model is based on the effective stress principle. Gravity is considered, and pore fluid pressure is formulated in terms of total pore pressure. We use the commercial software package ABAQUS for the FE calculations.

We use the northwest African continental slope as a prototype field location, as it can be regarded as a reasonably typical passive continental margin with low sediment input [*Weaver et al.*, 2000]. Off northwest Africa the continental shelf edge is at a water depth of 100–200 m [*Wynn et al.*, 2000]. The continental slope is 50–250 km long; sedimentation rate is typically highest along the shelf and decreases toward the deep sea [*Ruddiman et al.*, 1988]. Hemipelagic clay is the prevailing sediment type.

2.2.1. Model Geometry and Mesh

Most passive continental margins are reasonably uniform over large distances, so that two-dimensional modeling is adequate. The FE model comprises shelf, slope, and continental rise (Figure 3). The slope is 100 km long and dips at an angle of 2°. Although the main focus is on the slope and the upper 500 m below seafloor, the overall model area is bigger in order to avoid boundary effects. The FE mesh is finest within the upper 100 m of the model with 10 m long and 10 m wide elements. Between model depths of 100 m and 500 m the element size gradually increases to 100 m length and width. Outside the area of interest, at model depths larger than 500 m, the elements increase in size up to 1000 m at the model's basal boundary. The total number of elements is ~250,000. Boundary conditions are given in Figure 3.

2.2.2. Modeling Sedimentation

At the prototype field location off northwest Africa, *Ruddiman et al.* [1988] document maximum sedimentation rates of 0.15 m/kyr at the upper slope and 0.1 m/kyr at the midslope during the past 6 Ma. The rate of
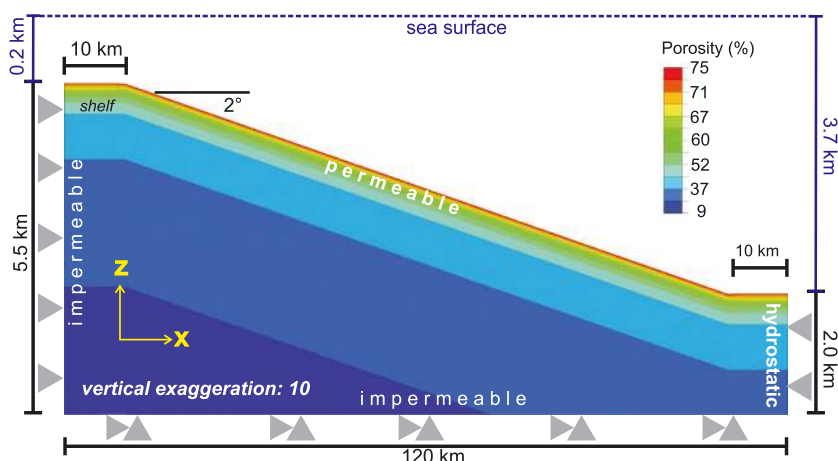
Figure 3. Two-dimensional model geometry (not to scale) representing a simplified but typical continental slope. Color coding represents the initial porosity distribution. Displacement boundary conditions are indicated by grey triangles. The lateral boundaries of the model are fixed against movements in the horizontal direction but are free to move vertically. The base of the model is fixed in both vertical and horizontal directions. The upper boundary is free to move in either vertical or horizontal direction. The landward boundary of the model (left side) is impermeable because loading due to sedimentation to both sides of this boundary is assumed equal and purely vertical flow is therefore expected. Pore fluid is allowed to flow through the abyssal plain boundary (right side). No flow takes place through the basal boundary as sediments at this depth are highly lithified and assumed to be virtually impermeable. See the text for details on the flow boundary condition at the model surface.

decrease from the shelf break to the toe of the slope is calculated from thinning rates of seismic sequences at various locations off northwest Africa. These rates of hemipelagic accumulation are consistent with those calculated from dated sediment cores, which penetrate the upper few meters of hemipelagic sediment [*Frenz et al.*, 2009]. We use the two end-member thinning rates to convert into two exponential equations that prescribe the decay of sedimentation rate downslope (smooth load S and localized load L, Figure 4a). Sedimentation rates over time can be constant or episodic (loads C and E, Figure 4b).
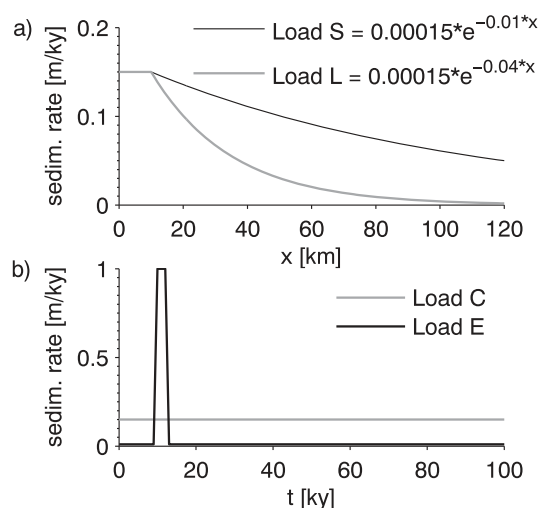

Figure 4. Spatial and temporal load distributions used in the 2-D finite element model expressed as sedimentation rates. (a) Two different spatial load distributions (S, L) with *x* as horizontal distance along the model domain. Both load distributions decline exponentially from the shelf and are based on thinning rates calculated from seismic sections. (b) Loading over time may either be constant (C) or episodic (E). When load E is applied the major part of the sediment is deposited within 2 kyr of model time.

Sedimentation as such is not implemented in the model. The newly added sediment itself is not physically modeled but simulated by an equivalent vertical load on the seafloor (Figure 5). This pressure load increases continuously over time, simulating the sediment deposited since the start of the model run, with a rate governed by the respective load distribution. As a consequence, the model surface does not represent the seafloor anymore for $t > 0$ (Figure 5). The conversion of sedimentation rate (thickness per unit time; m/kyr) into loading rate (pressure per unit time; kPa/kyr) is based on a porosity and dry density typical of seafloor sediments ($n = 70\%$, $\rho_{dry} = 780$ kg/m^3). As such, 0.15 m/kyr is equivalent to 1.8 kPa/kyr. For simplicity, the newly deposited sediment is referred to as "virtual layer" hereafter. The implications of this method are discussed below.

Due to the presence of the virtual layer, flow out of the model's surface cannot take place freely after deposition has started but is prescribed by

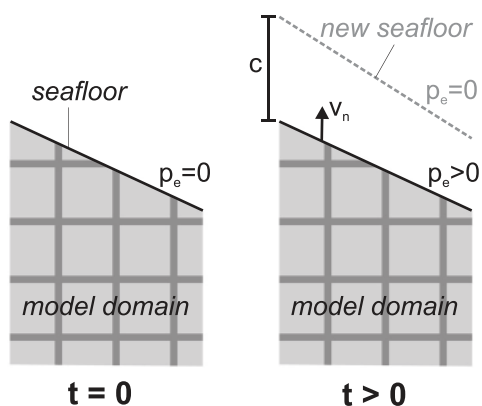$$v_n = \frac{k_{vl}}{\gamma_w \cdot c} \cdot (p - p_h). \quad (3)$$

Figure 5. Sketch of the surcharge method applied in the 2-D finite element model. Before simulation starts ($t = 0$) the model surface represents the seafloor, where excess pore pressure, p_e, is zero. In the model run accumulation of sediment is simulated by a vertical pressure load, the magnitude of which equals the weight of a layer of sediment that would have been accumulated under the prevailing sedimentation rate. Therefore, for $t > 0$ the model surface no longer represents the seafloor but is buried under a "virtual" sediment layer of thickness c. Fluid flow out of the model surface, v_n, is a function of c, the pore pressure gradient across the virtual layer, and permeability in the virtual sediment layer.

Here p is the current pore pressure at the model surface provided by the simulation itself, and p_h is the hydrostatic pore pressure at the new seafloor. The average permeability in the virtual layer, k_{vl}, equals the permeability at the model surface and decreases accordingly over time. The thickness of the virtual layer, c, is the product of sedimentation rate and model time for a given load distribution and distance along the x axis (Figure 4). The boundary condition including all required input parameters are updated at every numerical increment and every surface element.

Sedimentation rates are often estimated as the ratio of sediment thickness to time without a correction for a compaction-induced porosity change. Consequently applying these sedimentation rates in our model results in a too low thickness of the virtual layer. However, our numerical tests showed that variations in permeability or thickness of the virtual layer have only minor impacts on flow patterns in the uppermost row of elements.

2.2.3. Initial Conditions

To estimate the initial pore pressure, we follow the approach of *Viesca and Rice* [2012] described in section 2.1. Initial void ratio is inferred from the constitutive model ($e = 3.0$ at 1kPa), the respective mechanical properties, and effective pressure. All material points lie on the normal consolidation line with a coefficient of lateral earth pressure $K_0 = 0.6$. The initial size of the yield surface is determined such that the stress state lies on the yield surface.

2.2.4. Constitutive Model and Material Properties

Hemipelagic sediments are generally soft, highly sensitive, and fit within the critical state framework [*Baudet and Ho*, 2004; *Brandes*, 2010]. Hence, Modified Cam Clay [*Roscoe and Burland*, 1968] is an appropriate plasticity model. The amount of inelastic volume change determines the change in yield locus size according to an exponential strain hardening law. The plastic strain direction is defined by an associated flow rule. The elastic behavior is modeled with a nonlinear, isotropic porous elastic constitutive model. Nonlinear permeability is implemented as a function of porosity. Cohesion is zero for normally consolidated clays and silts [*Powrie*, 2002].

The friction angle at critical state, ϕ'_{crit}, for fine-grained hemipelagic sediment is often given as 30° [*Valent et al.*, 1982; *Kayen and Lee*, 1991; *Baraza et al.*, 1992; *Dugan and Germaine*, 2008]. The slope of the critical state line in the p'-q plane, M, is related to ϕ'_{crit} by $M = \frac{\sin \phi'_{crit} \cdot 6 \cdot \sqrt{1-b+b^2}}{3+\sin \phi'_{crit} \cdot 2 \cdot b - \sin \phi'_{crit}}$. For plane strain conditions $b = 0.5$ [*Powrie*, 2002] so that M=0.866.

The slope, λ, of the critical state line when projected onto the $v - \ln p'$ [kPa] space (with v as the specific volume and p' as effective pressure) determines the compressibility. Values for λ are highly variable, with an average upper limit 0.25 for hemipelagic sediments [*Valent et al.*, 1982; *Demars*, 1982; *Bayer and Wetzel*, 1989; *Leynaud et al.*, 2007; *Dugan*, 2008; *Schneider et al.*, 2009]. The elastic logarithmic bulk modulus, κ, is commonly estimated as $1/10$ of λ [*Powrie*, 2002] and is 0.025 in all models.

Permeability, k, is a function of porosity, n. We use the porosity-permeability relationship given by *Flemings et al.* [2012] for hemipelagic mud (equation (2)). A higher horizontal (k_x) than vertical permeability (k_z) with an anisotropy ratio of 10 is applied, which has been measured, for example, on mudstone samples from the Gulf of Mexico [*Reece et al.*, 2012]. To account for heterogeneities, such as the presence of fabric, fissuring, or fracturing, that allow for sideways drainage, we also use $k_x/k_z = 1000$ in one model run [*Clayton et al.*, 1995].

Dry density is a linear function of porosity (ρ_{dry}[kg/m^3] $= 2600(1 - n)$) and remains constant during the analysis. The specific weight of water is $\gamma_w = 10.24$ kN $\cdot$ m^{-3}. The sediment is fully saturated.

2.2.5. Layer

Layers of distinct material act as fluid pathways or barriers and may cause distinct flow patterns in a continental slope [*Dugan and Flemings*, 2000]. We therefore simulate continental slopes with a layer of distinct hydromechanical properties. The layer in our model is 20 m thick and extends over the entire length of the model. Both the upper and lower boundaries of the respective layer are permeable so that fluid can flow freely across the material interface.

To account for a fluid pathway (aquifer), the layer has a higher permeability than the background material, i.e., that of silty clay. The material's mechanical behavior is simulated with a nonlinear, isotropic porous elastic constitutive model. The elastic bulk modulus, κ, is 0.05, and Poisson's ratio, ν, is 0.3. Dry density is constant throughout the layer at 1100 kg/m³. The permeability of the silty clay layer is constant and anisotropic with $k_x/k_z = 10$. Vertical permeability, k_z, is 10^{-8} m/s. In other models the permeability (compressibility) of the layer is reduced (increased) stepwise to identify the critical values required for slope failure. All other material properties are taken identical to those of the surrounding material.

2.2.6. Assumptions and Limitations

Newly deposited sediment only provides a surface load in the models. Consequently, the model is not capable of simulating failure within this interval of newly deposited sediment. However, the main failure surfaces of the very large volume landslides on low-gradient seafloor addressed in this study are mostly 100 m to 250 m below seafloor [*Hühnerbach et al.*, 2004] (Figure 1b). Our method is thus applicable if the thickness of the newly deposited sediment is less than 100 m to 250 m, which is the case for the low accumulation rates and timescales considered here.

Compaction and pore fluid generation within the newly deposited sediment would occur in nature but are not simulated here. However, we assume that excess pore fluid generated above the failure surface is not relevant for the actual failure process, as the excess fluid will drain upward toward the seafloor or sideways. The processes responsible for slope failure rather act at or underneath the failure surface. Pore fluid generation above the failure surface can thus be neglected.

For all models small strain theory is used to reduce computational costs. This is known to overestimate excess pore pressures [*Gibson et al.*, 1981; *Schiffman et al.*, 1984], which can be crucial for geotechnical design analyses. The aim of this study, however, is to investigate fundamental processes and sensitivities in a qualitative manner. Moreover, this systematic error affects all models equally so that the results of models obtained using small strain analysis can be confidently compared.

The model does not account for thermal expansion of water and dehydration of clays. Although these factors can contribute to overpressure, they are not of importance for shallow sediments [*Chamley*, 1989; *Wangen*, 2000].

3. Results: 1-D Sedimentation-Consolidation Analysis

We use the 1-D sedimentation-consolidation analysis described in section 2.1 to calculate overpressure generated in a 500 m thick sediment column with an inclination of 2° undergoing sedimentation at a rate of 0.15 m/kyr and consolidation. Our aim is to identify values of permeability and compressibility that result in an overpressure ratio equal to or larger than 0.9, which has been identified as the level of overpressure necessary to cause failure of a 2° slope (Figure 2).

The parametric analysis shows that the porosity-permeability relationship has to be 500 times lower than that in the reference model (equation (2)). The critical compressibility, λ, required for causing an overpressure ratio $>= 0.9$ is 0.35. Figure 6 shows results for these analyses including a reference analysis with permeability and compressibility typical for fine-grained hemipelagic sediment.

The permeability, k, in the reference analysis (black curves in Figure 6a) decreases from $4 \cdot 10^{-9}$ m/s at the surface to $6 \cdot 10^{-10}$ m/s at 500m sediment depth. As expected, the curve of the low permeable sediment (green curves in Figure 6a) has an identical shape because the same porosity-permeability relationship is used but is shifted to lower values. In contrast, in the highly compressible sediment (blue curves in Figure 6a) the absolute decrease in permeability is much higher, falling from $4 \cdot 10^{-9}$ m/s at the seafloor down to $2 \cdot 10^{-13}$ m/s at 500 m.

The coefficient of consolidation, c_v, is an effective way to present the sediment's hydromechanical parameters controlling overpressure (Figure 6b). In the reference sediment this coefficient sharply increases from
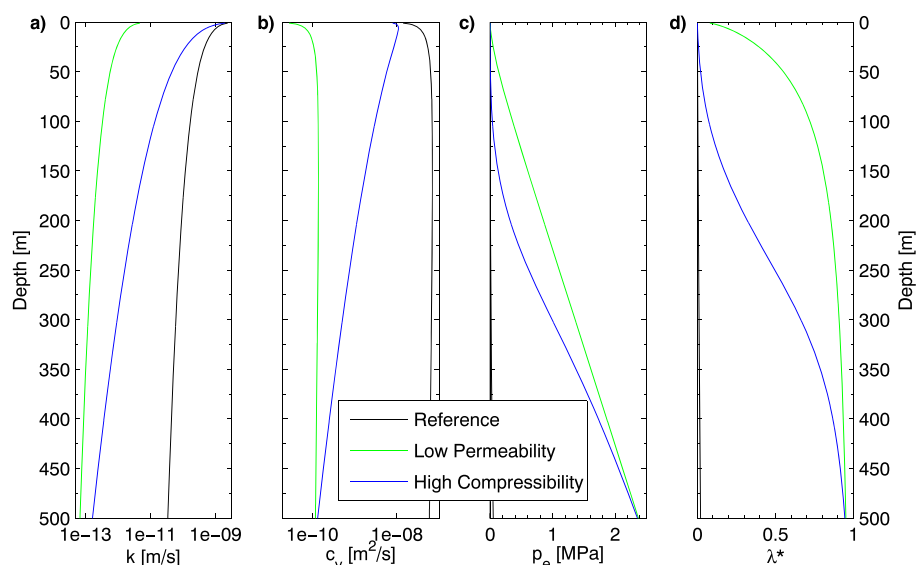
Figure 6. Sedimentation-consolidation analysis for a 500m thick hemipelagic sediment column of typical hydromechanical properties (reference analysis, black curves), low permeability (0.002·equation (2), green curves), and high compressibility ($\lambda = 0.35$, blue curves). Results are shown in terms of (a) permeability, k; (b) coefficient of consolidation, c_v; (c) excess pore pressure, p_e; and (d) overpressure ratio, λ^*.

$10^{-7.7}$ m^2/s at the top to a maximum of $10^{-7.1}$ m^2/s in 150 m before decreasing slowly toward a larger depth. In low permeable sediment we observe the same pattern with a minimum c_v of $3 \cdot 10^{-11}$ m^2/s at the surface and a maximum of $2 \cdot 10^{-10}$ m^2/s at 150 m. In rapidly compressing sediment the maximum c_v value, $c_v = 11 \cdot 10^{-9}$ m^2/s, locates much shallower with a steeper decline to $1 \cdot 10^{-10}$ m^2/s.

Excess pore pressures generated in the reference analysis (Figure 6c) are too low to have a significant effect on the stability of a low-angle slope. In contrast, a very low permeability as well as a high compressibility generates excess pore pressures up to 2.4 MPa in 500 m sediment depth. In a low permeable sediment excess pore pressure increases almost linearly from top to bottom, indicating that consolidation takes place almost independently of sediment depth. For a sediment of high compressibility p_e builds up more slowly in the upper 200 m. Farther downward, a higher gradient prevails, which causes a comparatively rapid rise in excess pore pressure below 200 m. More shallow parts of the sediment have the potential to consolidate faster, "locking" excess pore pressures in for shorter periods of time than deeper parts.

While an overpressure ratio of 0.9 is not reached in the reference scenario, in low permeable sediment this critical value is crossed at 280 m below seafloor and in highly compressible sediment at 350 m (Figure 6d). While the low permeable sediment shows a comparatively rapid increase in overpressure ratio in the upper 100 m rising from 0 to 0.7, the rate of increase below this depth is smaller. In contrast, the development of the overpressure ratio with depth for a rapidly compressing sediment is characterized by a slow increase in 0–200 m depth, followed by a zone of rapid increase between 200 and 400 m. This reflects different consolidation rates also observed in the excess pore pressure curves (Figure 6c).

The 1-D sedimentation-consolidation analysis showed that permeability or compressibility has to be extreme for significant overpressure to be generated when low sedimentation accumulation (0.15 m/kyr) is the only pressure source. Another generalization that may be made from this analysis is that rapidly compressing sediment accommodates overpressure at greater depths than low permeable sediment.

4. Results: 2-D FE Models

Assessing the effect of critical state friction angle, different loading scenarios, and permeability or compressibility contrasts on overpressure and slope stability requires two-dimensional FE models (section 2.2). First, results for a reference model run of a slope made of a single material with properties typical for fine-grained hemipelagic sediment are presented (Table 1). Variations to this reference model run, in which the load, permeability anisotropy, and critical state friction angle are modified one at a time, as well as models with layers

Table 1. Input Parameters for FE Models[a]

	λ	k_z	k_x/k_z	ϕ'_{crit}	Load	Layer	Figure
Reference model	0.25	equation (2)	10	30°	S/C	no	7
Localized load	0.25	equation (2)	10	30°	*L/C*	no	8a
Episodic load	0.25	equation (2)	10	30°	*S/E*	no	8b
Permeability anisotropy	0.25	equation (2)	*1000*	30°	S/C	no	8c
Friction angle	0.25	equation (2)	10	*10°*	S/C	no	8d
Highly permeable layer	0.25 (na)	equation (2) (10^{-8} m/s)	10	30°	S/C	*yes*	9a
Low permeable layer	0.25	equation (2) (equation (2) · 0.001)	10	30°	S/C	*yes*	9b
Highly compressible layer	0.25 (0.45)	equation (2)	10	30°	S/C	*yes*	9c and 10

[a]Column 2: Logarithmic bulk modulus (or compressibility), λ. Column 3: Porosity-permeability relationship, k_z. Column 4: Permeability anisotropy, k_x/k_z. Column 5: Critical friction angle, ϕ'_{crit}. Column 6: Load distribution (S = smooth, L = localized, C = constant, and E = episodic), compare Figure 4. Italic prints highlight parameters different to reference model. Numbers inside parentheses for models with layer give parameter values for material in that layer if it differs from the surrounding material, or not applicable (na), where a different soil model is used.

(Table 1), are presented in less detail. The results are shown in terms of excess pore pressure, p_e; overpressure ratio, λ^*; vertical effective stress, σ'_v; and the Factor of Safety (FOS). FOS is the ratio of available strength to mobilized shear strength and is calculated for each numerical integration point.

All model runs presented here considered continuous loading over a period of 1 Myr. After loading started, the model's surface no longer represents the seafloor, but a buried bedding plane. The depth of burial depends on the load distribution. After 1 Myr with load S (Figure 4a), 150 m of virtual sediment will have been deposited at the shelf and 50 m at the downslope end of the model. For load L (Figure 4b) the burial depth at the toe of the slope is 2.5 m. Failure and excess pore fluid generation are not simulated in the virtual layer between the model surface and the new seafloor. Nevertheless, failure depth are expected in 100 m to 250 m burial depths [*Hühnerbach et al.*, 2004] (Figure 1b).

4.1. Reference Model
Figure 7 shows simulation results for the reference model run with constant sediment load at a maximum rate of 0.15 m/kyr at the shelf (Table 1). Excess pore pressure increases continuously over time and with depth (Figures 7a and 7b). However, excess pore pressure rises at a very low rate, so the slope will most likely remain stable even if sediment deposition would continue over a period longer than 1000 kyr. The overpressure ratio at $t = 0$ kyr has maximum values at greatest depth, a trend which continues over time (Figure 7c). Maximum λ^* values are 0.3 in sediment depth >3 km. In depths more likely affected by landslides (<500 m), excess pore pressure takes up less than 6% of the lithostatic stress, which is insufficient to cause failure. Vertical effective stress increases over time and with depth, suggesting that the slope is very stable (Figures 7e and 7f). FOS does not fall below 2 at any time. It increases with increasing surcharge (Figures 7g and 7h), indicating that the slope becomes more stable over time.

4.2. Spatial and Temporal Loading Patterns
The localized deposition of sediment (Figure 8a) results in a very stable slope, similar to the reference model. In contrast, episodically high deposition rates (Figure 8b) may generate excess pore pressure, p_e, up to 1000 kPa and overpressure ratios >0.2. These maximum pore pressures, however, start to dissipate once the episode of high load terminates at $t = 12$ kyr. At the end of the analysis ($t = 1000$ kyr) all shown parameters at $x = 16$ km are almost identical to those in the reference model.

4.3. Permeability Anisotropy and Critical Friction Angle
If permeability anisotropy is very high, the maximum excess pore pressure at a depth of 500 m is less than 200 kPa and thus half of the maximum predicted by the reference model (Figure 8c). This indicates that sideways drainage is allowed by the higher lateral permeability. However, we do not observe any indications for destabilization farther downslope where the overburden is smaller (cf. *Dugan and Flemings* [2000], who modeled higher sedimentation rates).

Excess pore pressures generated by depositing sediment at a rate of 0.15 m/kyr are not sufficient to cause failure even when the sediment is very weak ($\phi'_{crit} = 10°$, Figure 8d). The Factor of Safety is lower than in
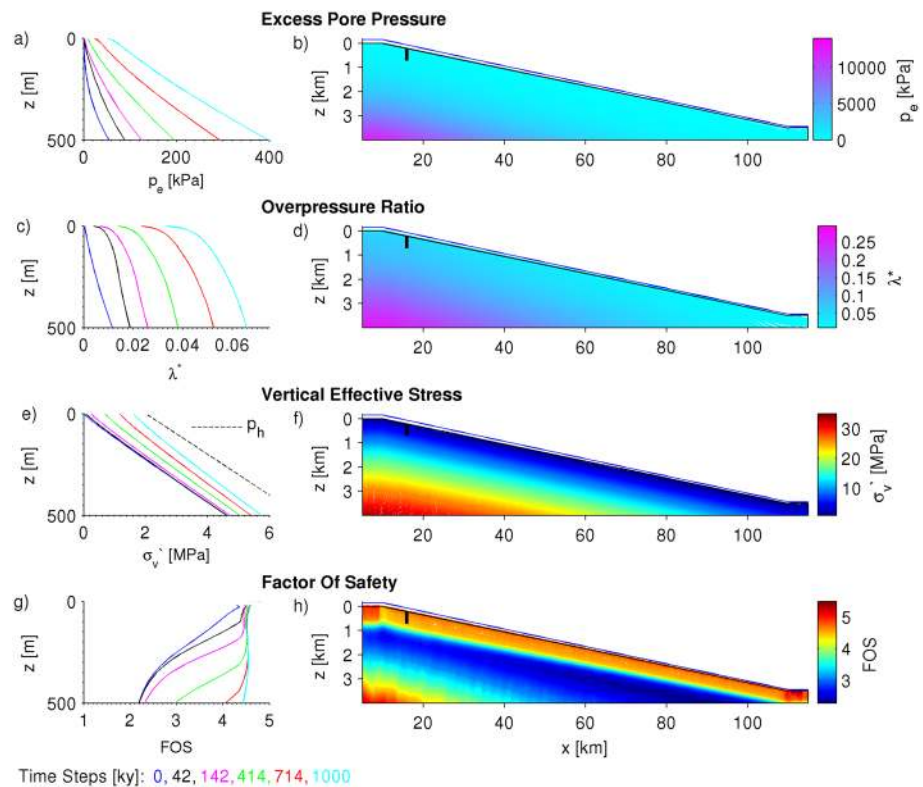
Figure 7. Results of the 2-D finite element consolidation analysis for the reference model run with typical physical-mechanical properties for hemipelagic sediment listed in Table 1. (a, c, e, and g) A vertical profile from the model surface to a model depth of 500 m at $x = 16$ km for several simulation time steps represented by different colors (color coding is given at the bottom of the figure). (b, d, f, and h) The location of the vertical profile is marked by a vertical black line. For $t > 0$ kyr the model surface no longer represents the seafloor but is buried under a continuously growing virtual sediment layer that reaches a thickness of 128 m at $t = 1,000$ kyr. Figures 7b, 7d, 7f, and 7h show the entire model domain after 1000kyr of loading, with the blue line delineating the top of the virtual sediment layer, i.e., the new seafloor. The grey dashed line in Figure 7e shows the hydrostatic pore pressure (p_h) profile. Note vertical exaggeration.

any of the previous models but, nevertheless, increases with time (Figure 8d-4), indicating that continuing sedimentation has a stabilizing effect.

4.4. Layers

For the models including a 20m thick layer of different hydromechanical properties, we plot the temporal evolution of the stability-related parameters in a vertical profile of the upper 100 m of the model at $x = 16$ km. We test whether a high-permeability layer allows for lateral drainage causing failure away from the load maximum and identify the critical permeability and compressibility of the layer required for slope failure.

4.4.1. Layer of High Permeability

In the upper 100 m of the model with a layer of high permeability, excess pore pressure increases continuously over time and with depth to a maximum of 90 kPa (Figure 9a-1). Within the layer excess pore pressure does not increase with depth, but the vertical effective stress does, causing a decrease in the overpressure ratio λ^* (Figures 9a-2 and 9a-3). Nowhere in the model and at no time increment do λ^* exceed 0.1. At the end of the analysis the highest values (λ^*=0.04) are encountered at the top of the layer. This means that the FOS is everywhere >1 and increases with time (Figure 9a-4). We conclude that a high-permeability layer allows for lateral drainage in our model but does not cause failure away from the load maximum.

4.4.2. Layer of Low Permeability

We found that in order to generate sufficient overpressure to destabilize the slope, the layer needs to have a permeability that is 3 orders of magnitude lower than that of the surrounding sediment (Figure 9b). While above the layer excess pore pressure does not exceed 50 kPa, it rapidly increases within the layer (Figure 9b-1). Below the layer values increase at depth with a less steep gradient. At the end of the analysis p_e at the bottom of the layer has risen to 1500 kPa. The highest overpressure ratio ($\lambda^* = 0.8$) develops at the interface between
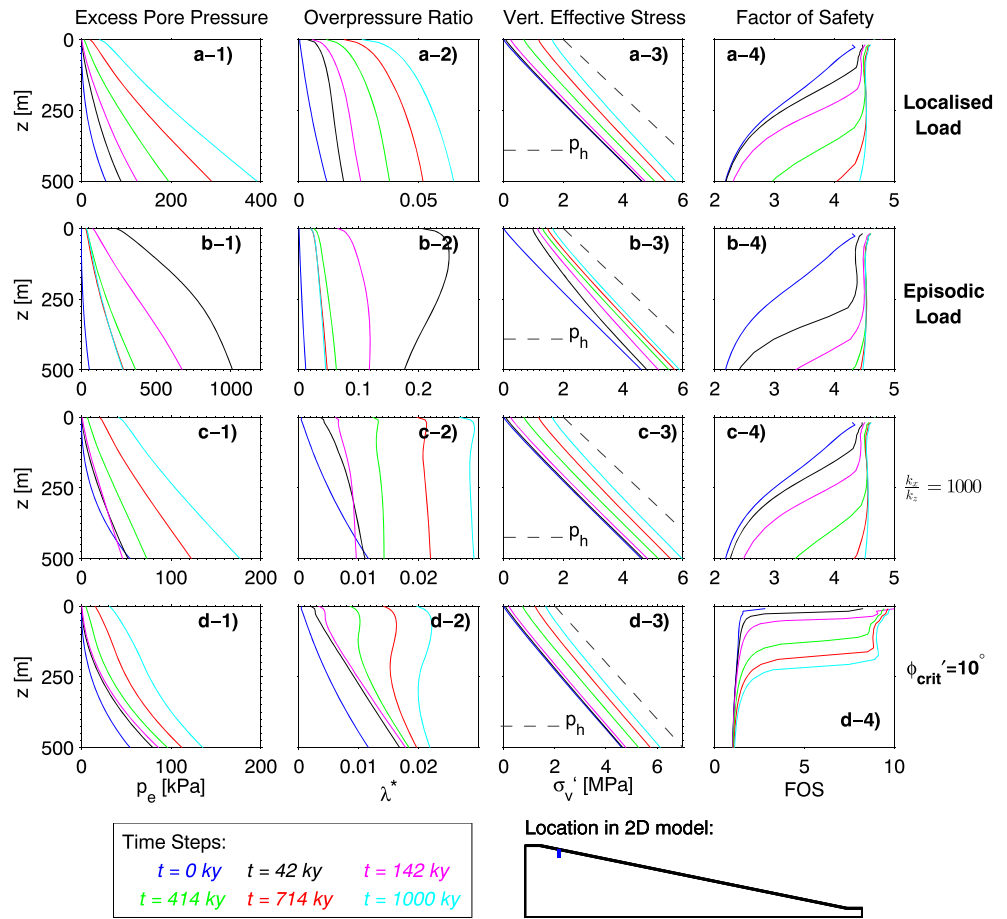
Figure 8. Vertical profiles for 2-D FE consolidation models that differ in one parameter from the reference model run shown in Figure 7 (see Table 1): (a) Model run with constant, localized load; (b) model run with episodic load; (c) model run with sediment of high-permeability anisotropy ($kx/kz = 1000$); and (d) model run with weak sediment ($\phi'_{crit} = 10°$). Vertical profiles from the model surface to a model depth of 500m at $x = 16$ km are shown for several simulation time steps represented by different colors. Color coding as well as the location of the vertical profiles in the model domain are given at the bottom of the figure. For $t > 0$ kyr the model surface no longer represents the seafloor but is buried under a continuously growing virtual sediment layer that after $t = 1,000$ kyr of sediment deposition reaches a thickness of 118 m in Figure 8a and 128m in Figures 8b–8d. The graphs show the evolution over time of excess pore pressure, p_e, (Figures 8a-1, 8b-1, 8c-1, and 8d-1); overpressure ratio, λ^*, (Figures 8a-2, 8b-2, 8c-2, and 8d-2); vertical effective stress, σ'_v, with hydrostatic pore pressure profile (Figures 8a-3, 8b-3, 8c-3, and 8d-3); and Factor of Safety, FOS, (Figures 8a-4, 8b-4, 8c-4, and 8d-4).

the low-permeability layer and the underlying sediment. While λ^* increases rapidly from the start until about 414 kyr (green markers in Figure 9b-2), its rate of increase is much lower in the last 500 kyr. In line with this, vertical effective stress at the bottom interface of the layer decreases in the first half of the modeled time frame but increases afterward (Figure 9b-3). The Factor of Safety increases from $t = 0$ kyr to $t = 142$ kyr and decreases again afterward. It is lowest just below the layer (FOS = 2.5) at $t = 714$ kyr (red marker in Figure 9b-4) but increases again toward the end of the analysis (cyan markers). Although stability below the layer is greatly reduced, we do not observe failure.

4.4.3. Layer of High Compressibility

Figure 9c shows simulation results for a model with a highly compressible layer. The compressibility of the layer is $\lambda = 0.45$, which is the minimum value that can lead to the generation of sufficiently high overpressure to cause failure of a 2° slope. Excess pore pressure increases with a steep gradient from the top to the bottom of the layer (Figure 9c-1). Fluid flow below the layer is horizontal (Figure 9c-1). The highest overpressure ratio ($\lambda^* = 0.9$) develops at the bottom of the layer (Figure 9c-2) and decreases below the layer. Overpressure ratio continuously rises with time. This pattern is also expressed in the vertical effective stress, which decreases with time at the bottom of the layer and approaches zero at 1000kyr (Figure 9c-3). In this area, FOS falls below 1 at
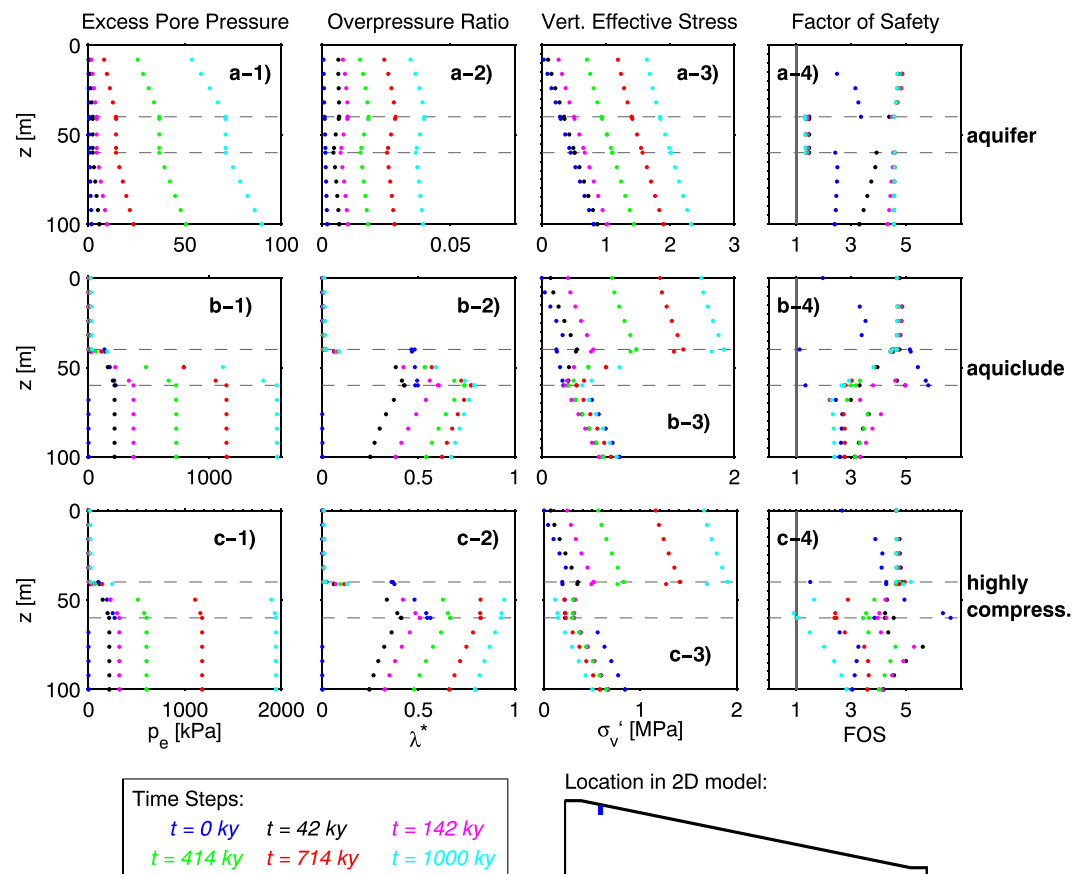
Figure 9. Vertical profiles for 2-D FE consolidation models for three models including layers of different properties than the surrounding material (see Table 1): (a) Highly permeable silty clay layer (aquifer), (b) low-permeability layer with permeability being 1/1000 of the surrounding material (aquiclude), and (c) highly compressible layer with $\lambda = 0.45$. Vertical profiles from the model surface to a model depth of 500 m at $x = 16$ km are shown for several simulation time steps represented by different colors. Color coding as well as the location of the vertical profiles in the model domain is given at the bottom of the figure. For $t > 0$ kyr the model surface no longer represents the seafloor but is buried under a continuously growing virtual sediment layer that after $t = 1000$ kyr of sediment deposition reaches a thickness of 128m. The graphs show the evolution over time of excess pore pressure, p_e, (Figures 9a-1, 9b-1, and 9c-1); overpressure ratio, λ^*, (Figures 9a-2, 9b-2, and 9c-2); vertical effective stress, σ'_v, (Figures 9a-3, 9b-3, and 9c-3), and Factor of Safety, FOS, (Figures 9a-4, 9b-4, and 9c-4).

$t = 1000$ kyr (Figure 9c-4). Indeed, incremental displacements indicate an approximately 5km long failure surface developing at the base of the layer (Figure 10a). The stress paths of several numerical integration points show that a block of material between 52m and 58m reached critical state, and hence failure (Figure 10b). Below this depth the material is very close to failure. A landslide would remove all sediments above and within the layer.

4.5. Summary of Modeling Results

There are no indications for instability or the onset of landsliding in the simulations, except in those including layers of extremely low permeability or very high compressibility. Failure occurred only in the latter, although the slope was brought close to failure by the former. Neither the spatial distribution of sedimentation nor a short episode of high sediment accumulation has a significant effect on the stability of the slope. Driving forces for slope failure are too small even for very weak sediment. A strong permeability anisotropy as well as the presence of a high-permeability layer allows for lateral drainage into areas of lower overburden, which increases slope stability.

We identified critical permeability and compressibility values that enable continental slope sediment to generate high overpressure. We do this for situations, where the rate of deposition is as low, i.e., 0.15 m/kyr. Permeability needs to be 500 times lower than that measured for hemipelagic mud. Compressibility, or the
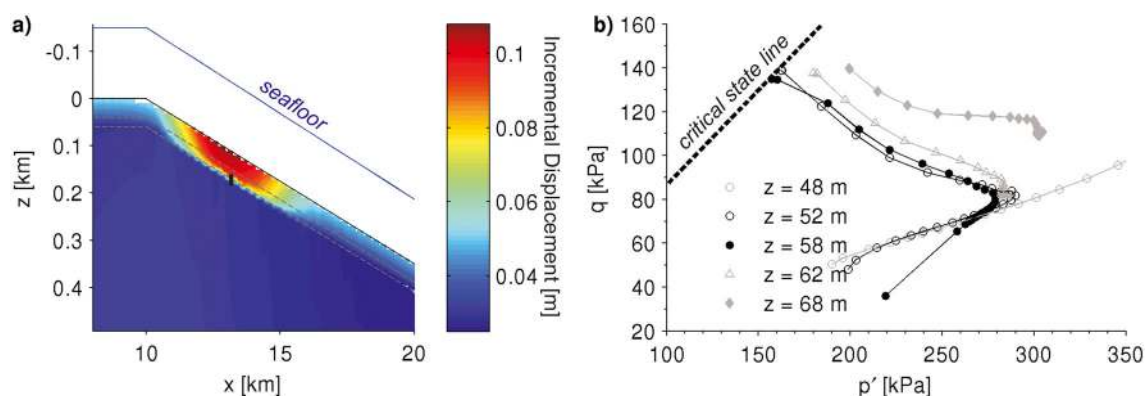
Figure 10. Indications for slope failure in the model with a highly compressible layer: (a) Close-up of the failing part of the model showing incremental total displacement in the last 3 kyr. The dashed grey lines delineate the layer boundary and the blue line the new seafloor. The black line at $x = 13$ km marks the location of integration points shown in the right panel. (b) Effective stress paths in a plot of deviator stress, q, versus effective pressure, p', for numerical integration points within the highly compressible layer ($z < 60$ m below model surface) and underneath it ($z > 60$ m). The dashed black line shows the corresponding critical state line. Failure occurs when the stress paths crosses the critical state line, which is the case at the bottom of the layer (52–58 m). The sediment underneath the layer is close to failure (62–68 m).

slope of the critical state line when projected onto the $v - \ln p'$ space (λ), has to be as high as 0.35. When a 20 m thick layer of different material properties is introduced, permeability in this layer must be more than 1000 times lower than that of hemipelagic mud. A 20 m thick silty clay layer that has relatively high permeability tends not to cause failure. The critical compressibility for generating sufficiently high overpressure is 0.45. However, these critical values for permeability and compressibility should be taken as a first approximation. Different initial conditions, such as the initial porosity or the profile of initial excess pore pressure, will lead to different results.

5. Discussion

It takes overpressure ratios greater than 0.9 to destabilize a 2° slope (Figure 2). Our modeling results show that such high excess pore pressures are difficult to generate in areas of slow (0.15 m/kyr) sediment accumulation, such as offshore northwest Africa. The loading provided by such slow sediment deposition is neither rapid enough to cause significant excess pore pressure where overburden is high nor to induce enough fluid flow or pressure transfer toward areas of lower overburden to decrease stability at the toe of the slope. Only where consolidation properties are extreme can sufficiently high overpressure be generated. In the following we discuss whether these extreme properties are realistic and for what sediment type they may be expected.

5.1. Permeability

Considering a slope of uniform material, permeability be must be less than 10^{-11} m/s at the seafloor and 10^{-13} m/s at 500 m depth. This is 500 times lower than the values measured for hemipelagic mud [*Flemings et al.*, 2012]. Thus, such low permeabilities seem unrealistic. Alternatively, the presence of a layer with permeability of 10^{-13} m/s, corresponding to one thousandth of the permeability-porosity relationship measured by *Flemings et al.* [2012] for hemipelagic mud, could also generate large overpressure. The minimum permeability values measured on offshore samples from 500m below seafloor do not fall below 10^{-12} m/s [e.g., *Reece et al.*, 2012; *Guo et al.*, 2013; *Daigle and Dugan*, 2014]. No data are known to us that indicate permeabilities needed to cause failure in our model than these for shallow (<200 m) deep sea sediments at low effective stresses.

5.2. Compressibility

If an entire slope is made up of a single type of sediment, its critical compressibility for causing significant overpressure is $\lambda = 0.35$. These overpressures can also be achieved with a layer of $\lambda = 0.45$ within a slope of typical hemipelagic mud. Compressibility depends on microstructure, which is governed by the conditions that prevail during deposition. On average, deep sea sediments are more compressible than typical terrestrial silts and clays. This is due to the more flocculated microstructures that can form in the ocean, owing to sedimentation through salt water and under very low accumulation rates [*Brandes*, 2010]. Although most λ values for deep sea sediments are below 0.25 [*Long et al.*, 2011; *Dugan*, 2008; *Veyera et al.*, 2001; *Berre et al.*, 1996], higher values have been measured on samples from particular sites and conditions. Organic-rich sediments from the Peru-Chile continental margin have $\lambda > 0.41$ [*Busch and Keller*, 1982]. The authors find the highest

compressibility (λ = 0.93) in samples from a mud lens with 12% organic carbon. In the Gulf of Guinea, *Hattab and Favre* [2010] measure λ values of up to 0.88 on samples from a smectite-rich clay with 6% organic content. Sedimentation rates in both areas are just slightly higher than in our prototype field location off northwest Africa: between 0.17 and 1.4 m/kyr [*Busch and Keller*, 1982] in the upwelling area of the Peru-Chile margin and about 0.3m/kyr in the Gulf of Guinea [*Pastouret et al.*, 1979]. Deep sea basin sediments from the Madeira Abyssal Plain, northeast Atlantic, and the Ulleung Basin, East Sea, exhibit λ values greater than 0.45 and large amounts of organic carbonate dominated by microfossils [*Brandes*, 2010; *Lee et al.*, 2011]. High compressibilities thus are not rare. Our modeling thus suggests that sediment with high compressibilities can potentially cause failure of very low gradient submerged slopes. We therefore now answer the question, what causes high compressibility in deep sea sediments?

5.2.1. Biogenic Silica

A process causing not only rapid compaction but also the liberation of bound water is the conversion of opal A into opal CT [*Eichhubl and Boles*, 2000; *Tada*, 1991]. This thermochemical dehydration reaction takes place during burial over geologically short time periods and large areas in sedimentary basins. However, successions enriched in biogenic silica occur only where primary production is high in equatorial regions and high latitudes. Moreover, the reaction front often locates 300–800 m below seafloor and is thus of importance for deep-seated failures only [*Volpi et al.*, 2003; *Davies and Clark*, 2006]. Therefore, diagenetic conversion of biogenic silica may not be a global and widespread source of overpressure. Substantial migration of pore fluid to much shallower depths would be needed.

5.2.2. Organic Content

Numerous authors [e.g., *Busch and Keller*, 1982; *Pusch*, 1973; *Keller*, 1982; *Booth and Dahl*, 1985; *Bennett et al.*, 1985] suggest a positive relationship between organic content and compressibility. The sensitivity of organic-rich sediments is of the order of 9, indicating a loss of strength of up to 90% once all natural internal structure has been disturbed and the sediment is in a remolded state. Corresponding beds may provide weak layers that could accommodate bedding-parallel slope failure either through the development of high excess pore pressure due to their high compressibility or the nearly complete loss of strength after an event capable of remolding the sediment, such as a strong earthquake. Sediments underlying highly productive coastal waters are particularly rich in organic matter, but the presence of such organic matter-rich clays is not limited to specific geological settings [*Premuzic et al.*, 1982]. It is therefore possible that such high compressibilities are more prevalent than reflected in the literature and may play an important role in destabilizing continental slopes. Intense primary production due to upwelling has dominated our prototype field location off northwest Africa [*Ruddiman et al.*, 1988]. It is therefore very likely that layers of high organic contents are present.

5.2.3. Loss of Structure

When high compressibilities are encountered, many authors also report high "apparent" overconsolidation ratios, in the absence of evidence for erosion that would explain the presence of overconsolidated sediment [*Richards and Hamilton*, 1967; *Bryant et al.*, 1974; *Busch and Keller*, 1982; *Keller*, 1982; *Wetzel*, 1990; *Cochonat et al.*, 1993; *Mulder et al.*, 1994; *Hattab and Favre*, 2010; *Guo et al.*, 2013]. A high overconsolidation ratio indicates that the sediment is capable of sustaining pressures greater than the overburden pressure at their original depth in the seabed without developing irreversible deformation. Where analyzed, it has been shown that apparent overconsolidation is often an effect of early cementation [*Won and Chang*, 2007; *Guo et al.*, 2013]. Cementation provides an internal structure that allows sediment to exist at a higher porosity. Such sediment does not compact to as low porosities at a given stress than a sediment without such structure [*Burland*, 1990]. Comparatively long timescales, as encountered in the marine realm, favor the development of early cementation and the buildup of a structural framework [*Skempton*, 1970] suggesting that sediments at continental margins may be highly structured. In the compaction process this initially stiff behavior, however, is followed by yield and the degradation of this structure, which is characterized by an increase in the rate of volume loss.

Crushing of microfossils during compaction is a process with similar effects on the compaction behavior and excess pore pressure generation as described above. Microfossils are relatively common in many hemipelagic muds. Their shells act as structural components that prevent the sediment from consolidating to as low porosities as other clays [*Hamilton*, 1976; *Keller*, 1982; *Tanaka and Locat*, 1999]. At some point during burial these shells cannot withstand the pressure and collapse, providing a high compressibility, sudden loss in volume, and, consequently, excess pore pressure generation [*Valent et al.*, 1982]. Indeed, an increase in microfossil content of a sediment correlates to an increase in compressibility [*Shiwakoti et al.*, 2002; *Hong et al.*, 2006]. Moreover, the expulsion of intraparticle water stored in hollow shells and skeletal pores could provide an

additional pore pressure source [*Demars*, 1982; *Keller*, 1982; *Hong et al.*, 2006]. *Palmer-Julson and Rack* [1992] and *Rack et al.* [1993] report intraparticle water in diatomaceous oozes as high as 15% of the dry weight.

Microfossils may also be locally cemented at their contacts, and these bonds can break. Particularly, unconsolidated sediments rich in carbonate show a high porosity even at larger depths [*Hamilton*, 1976; *Bryant et al.*, 1981] and can be comparably stiff (D. Masson, personal communication, 2012) (based on observations of white cemented hemipelagic muds in cores taken off northwest Africa). The absence of evidence for compaction in such sediments indicates that cementation begins early, before compaction due to major overburden by sediment accumulation [*Zankl*, 1969; *Bathurst*, 1971]. The cement at the grain boundaries can be considered an additional component of strength. As mechanical compaction due to overburden or shearing on a slope occurs, the cemented bonds may break, causing a rapid loss in strength and porosity. Besides calcium carbonate, other cementation agents are iron oxides, iron sulphides, and organic materials [*Bathurst*, 1971].

The loss of structure not only causes an increase in excess pore pressure due to the rapid loss of pore space but also induces a significant loss of strength, which provides the conditions for the material to move over long distances on low gradients. The particular type of sediment that maintains high porosities is likely deposited as a stratigraphic layer over long distances of the respective continental slopes. Failure will thus be bedding parallel over large areas. Hence, the loss of structure as a trigger mechanism agrees well with key characteristics shared by large submarine landslides globally and independently of their respective geological settings. The loss of structure could therefore be a global and widespread trigger for large submarine landslides.

6. Conclusion

Submarine landslides on open continental slopes are remarkable for their size and because they occur on slope angles of 2°. Previous modeling does not account for failures on such low gradients, in areas where sedimentation rates are slow (<0.15m/kyr), such as off northwest Africa. As landslides may produce damaging and far-traveling tsunamis, there is need for better understanding to improve hazard assessments and mitigation efforts. It has been suggested that rapid deposition of low permeable sediment can cause excess pore pressures in a continental slope that either directly causes failure or drives pore fluids into areas of less overburden at the toe of slope and causes failure there. We find that if deposition is slow (<0.15m/kyr), it is very difficult to generate overpressure or lateral fluid flow sufficient to destabilize or significantly weaken a low-angle slope. The hydromechanical properties of the sediment must be extreme and often take up values that to our knowledge have not been measured to date. Nevertheless, the presence of a layer that is either extremely rich in organic matter or that undergoes a rapid porosity decline has the potential to generate slope failure when slow sediment accumulation is the only pressure source.

Notation

γ_w specific fluid weight, kN/m^3.
κ swelling index, dimensionless.
λ logarithmic bulk modulus, dimensionless.
λ^* overpressure ratio, dimensionless.
v Poisson ratio, dimensionless.
ϕ'_{crit} effective angle of friction, °.
ρ_{dry} dry density, kg/m^3.
σ_v vertical stress, kPa.
σ'_v vertical effective stress, kPa.
M slope of critical state line, dimensionless.
E episodic loading rate, m/kyr.
E_0 Young's Modulus, kPa.
K bulk modulus, kPa.
K_0 coefficient of lateral earth pressure, dimensionless.
L localized loading rate, m/kyr.
S smooth loading distribution, m/kyr.
b parameter defining intermediate principle stress, dimensionless.
c thickness of virtual layer, m.

c_v	coefficient of consolidation, m^2/s.
e	void ratio, dimensionless.
e_0	void ratio at unity, dimensionless.
g	gravity acceleration, m/s^2.
k_{vl}	permeability of virtual layer, m/s,
k_x	horizontal permeability, m/s.
k_z	vertical permeability, m/s.
n	porosity, dimensionless.
p'	average principle effective stress, kPa.
p	pore pressure, kPa.
p_e	excess pore pressure, kPa.
p_h	hydrostatic pore pressure, kPa.
q	deviator stress, kPa.
v_n	fluid velocity normal to model surface, m/s.

References

Antobreh, A. A., and S. Krastel (2007), Mauritania Slide Complex: Morphology, seismic characterisation and process of formation, *Int. J. Earth Sci.*, *96*, 451–472, doi:10.1007/s00531-006-0112-8.

Baraza, J., G. Ercilla, and H. J. Lee (1992), Geotechnical properties and preliminary assessment of sediment stability on the continental slope of the northwestern Alboran Sea, *Geo-Mar. Lett.*, *12*, 150–156, doi:10.1007/BF02.084926.

Bathurst, R. G. (1971), *Carbonate Sediments and Their Diagenesis*, Elsevier, Amsterdam.

Baudet, B. A., and E. W. L. Ho (2004), On the behaviour of deep-ocean sediments, *Geotechnique*, *54*(9), 571–580, doi:10.1680/geot.2004.54.9.571.

Bayer, U., and A. Wetzel (1989), Compactional behavior of fine-grained sediments: Examples from Deep Sea Drilling Project cores, *Geol. Rundsch.*, *78*, 807–819, doi:10.1007/BF01.829324.

Bennett, R. H., L. Lehman, M. H. Hulbert, G. R. Harvey, S. A. Bush, E. B. Forde, P. Crews, and W. B. Sawyer (1985), Interrelationships of organic carbon and submarine sediment geotechnical properties, *Mar. Geotechnol.*, *6*(1), 61–98, doi:10.1080/10641198509388180.

Berre, T., M. Gutierrez, K. Høeg, N. Nagel, and T. Kristiansen (1996), Laboratory testing of an overburden shale, *Proceedings of the 5th North Sea Chalk Symposium*, Reims, France, 7–9 Oct.

Binh, N. T. T., T. Tokunaga, T. Nakamura, K. Kozumi, M. Nakajuma, M. Kubota, H. Kameya, and M. Taniue (2009), Physical properties of the shallow sediments in late Pleistocene formations, Ursa Basin, Gulf of Mexico, and their implications for generation and preservation of shallow overpressures, *Mar. Pet. Geol.*, *26*, 474–486, doi:10.1016/j.marpetgeo.2009.01.018.

Bondevik, S., F. Lovholt, C. Harbitz, J. Mangerud, A. Dawson, and J. I. Svendsen (2005), The Storegga Slide tsunami-comparing field observations with numerical simulations, *Mar. Pet. Geol.*, *22*(1–2), 195–208, doi:10.1016/j.marpetgeo.2004.10.003.

Booth, J. S., and A. G. Dahl (1985), A note on the relationships between organic matter and some geotechnical properties of a marine sediment, *Mar. Geotechnol.*, *6*(3), 281–289, doi:10.1080/10641198609388191.

Boyd, R., J. Keene, T. Hubble, J. Gardner, K. Glenn, K. Ruming, and N. Exon (2010), Southeast Australia: A Cenozoic continental margin dominated by mass transport, in *Submarine Mass Movements and Their Consequences, Advances in Natural and Technological Hazards Research,* vol. 28, edited by D. C. Mosher et al., pp. 491–502, Springer, Netherlands, doi:10.1007/978-90-481-3071-9_40.

Brandes, H. G. (2010), Geotechnical characteristics of deep-sea sediments from the North Atlantic and North Pacific oceans, *Ocean Eng.*, *38*(7), 835–848, doi:10.1016/j.oceaneng.2010.09.001.

Bryant, W. R., A. P. Delflache, and P. K. Trabant (1974), *Deep-Sea Sediments*, chap. Consolidation of marine clays and carbonates, pp. 209–244, Plenum, New York.

Bryant, W. R., R. H. Bennett, and C. E. Katherman (1981), *The Oceanic Lithosphere, The Sea*, vol. 7, chap. Shear strength, consolidation, porosity, and permeability of oceanic sediments, pp. 1555–1616, Wiley, New York.

Burland, J. B. (1990), On the compressibility and shear strength of natural clays, *Geotechnique*, *40*(3), 329–378, doi:10.1680/geot.1990.40.3.329.

Busch, W. H., and G. H. Keller (1982), Consolidation characteristics of sediments from the Peru-Chile continental margin and implications for past sediment instability, *Mar. Geol.*, *45*(1–2), 17–39, doi:10.1016/0025-3227(82)90178-5.

Chamley, H. (1989), *Clay Sedimentology*, 623 pp., Springer, Berlin.

Clayton, C. R. I., M. C. Matthews, and N. E. Simons (1995), *Site Investigation: A Handbook for Engineers*, 584 pp., Blackwell Science, Oxford, U. K.

Cochonat, P., J. F. Bourillet, B. Savoye, and L. Dodd (1993), Geotechnical characteristics and instability of submarine slope sediments, the nice slope (N-W Mediterranean Sea), *Mar. Georesour. Geotechnol.*, *11*(2), 131–151, doi:10.1080/10641199309379912.

Daigle, H., and B. Dugan (2014), Data report: Permeability, consolidation, stress state, and pore system characteristics of sediments from Sites C0011, C0012, and C0018 of the Nankai Trough, in *Proc. of the Integrated Ocean Drilling Program*, vol. 333, edited by P. Henry et al., Integr. Ocean Drill. Program Manage. Intl. Inc.,Tokyo, doi:10.2204/iodp.proc.333.201.2014.

Davies, R. J., and I. R. Clark (2006), Submarine slope failure primed and triggered by silica and its diagenesis, *Basin Res.*, *18*(3), 339–350, doi:10.1111/j.1365-2117.2006.00297.x.

Demars, K. R. (1982), Unique engineering properties and compression behavior of deep-sea calcareous sediments, in *Geotechnical Properties, Behavior and Performance of Calcareous Soils*, edited by K. R. Demars and R. C. Chaney, pp. 97–112, Am. Soc. Testing Materials, Philadelphia, Pa.

Dugan, B. (2008), Fluid flow in the Keathley Canyon 151 Mini-Basin, northern Gulf of Mexico, *Mar. Pet. Geol.*, *25*(9), 919–923, doi:10.1016/j.marpetgeo.2007.12.005.

Dugan, B., and P. B. Flemings (2000), Overpressure and fluid flow in the New Jersey continental slope: Implications for slope failure and cold seeps, *Science*, *289*, 288–291, doi:10.1126/science.289.5477.288.

Dugan, B., and P. B. Flemings (2002), Fluid flow and stability of the US continental slope offshore New Jersey from the Pleistocene to the present, *Geofluids*, *2*, 137–146, doi:10.1046/j.1468-8123.2002.00032.x.

Dugan, B., and J. T. Germaine (2008), Near-seafloor overpressure in the deepwater Mississippi Canyon, northern Gulf of Mexico, *Geophys. Res. Lett.*, *35*, L02304, doi:10.1029/2007GL032275.

Eichhubl, P., and J. R. Boles (2000), Focused fluid flow along faults in the Monterey Formation, coastal California, *Geol. Soc. Am. Bull.*, *112*(11), 1667–1679, doi:10.1130/0016-7606(2000)112<1667:FFFAFI>2.0.CO;2.

Flemings, P. B., B. B. Stump, T. Finkbeiner, and M. Zoback (2002), Flow focusing in overpressured sandstones: Theory, observations, and applications, *Am. J. Sci.*, *302*(10), 827–855, doi:10.2475/ajs.302.10.827.

Flemings, P. B., H. Long, B. Dugan, J. T. Germaine, C. M. John, J. H. Behrmann, D. E. Sawyer, and IODP Expedition 308 Scientists (2008), Erratum to "Pore pressure penetrometers document high overpressure near the seafloor where multiple submarine landslides have occurred on the continental slope, offshore Louisiana, Gulf of Mexico", *Earth Planet. Sci. Lett.*, *274*, 269–283, doi:10.1016/j.epsl.2008.06.027.

Flemings, P. B., C. John, and J. H. Behrmann (2012), Expedition 308 synthesis: Overpressure, consolidation and slope stability on the continental slope of the Gulf of Mexico, in *Proc. of the Integrated Ocean Drilling Program*, vol. 308, edited by P. B. Flemings et al., Integr. Ocean Drill. Program Manage. Intl. Inc., College Station, Tex., doi:10.2204/iodp.proc.308.215.2012.

Frenz, M., R. B. Wynn, A. Georgiopoulou, V. B. Bender, G. Hough, D. G. Masson, P. J. Talling, and B. T. Cronin (2009), Provenance and pathways of late Quaternary turbidites in the deep-water Agadir Basin, northwest African margin, *Int. J. Earth Sci.*, *98*(4), 721–733, doi:10.1007/s00531-008-0313-4.

Gibson, R. E. (1958), The progress of consolidation in a clay layer increasing in thickness with time, *Geotechnique*, *8*(2), 171–182, doi:10.1680/geot.1958.8.4.171.

Gibson, R. E., R. L. Schiffman, and K. W. Cargill (1981), The theory of one-dimensional consolidation of saturated clays. II. Finite nonlinear consolidation of thick homogeneous layers, *Can. Geotech. J.*, *18*(2), 280–293, doi:10.1139/t81-030.

Guo, J., M. B. Underwood, W. J. Likos, and D. M. Saffer (2013), Apparent overconsolidation of mudstones in the Kumano Basin of Southwest Japan: Implications for fluid pressure and fluid flow within a forearc setting, *Geochem. Geophys. Geosyst.*, *14*(4), 1023–1038, doi:10.1029/2012GC004204.

Haflidason, H., H. P. Sejrup, A. Nygard, J. Mienert, P. Bryn, R. Lien, C. F. Forsberg, K. Berg, and D. Masson (2004), The Storegga Slide: Architecture, geometry and slide development, *Mar. Geol.*, *213*, 201–234, doi:10.1016/j.marpetgeo.2004.10.008.

Hamilton, E. L. (1976), Variations of density and porosity with depth in deep-sea sediments, *J. Sediment. Petrol.*, *46*(2), 280–300.

Hampton, M. A., H. J. Lee, and J. Locat (1996), Submarine landslides, *Rev. Geophys.*, *34*, 33–59, doi:10.1029/95RG03287.

Hattab, M., and J.-L. Favre (2010), Analysis of the experimental compressibility of deep water marine sediments from the Gulf of Guinea, *Mar. Pet. Geol.*, *27*(2), 486–499, doi:10.1016/j.marpetgeo.2009.11.004.

Hong, Z., Y. Tateishi, and J. Han (2006), Experimental study of macro- and microbehavior of natural diatomite, *J. Geotech. Geoenviron. Eng.*, *132*, 603–610, doi:10.1061/(ASCE)1090-0241(2006)132:5(603).

Hornbach, M. J., L. L. Lavier, and C. D. Ruppel (2007), Triggering mechanism and tsunamogenic potential of the Cape Fear Slide complex, U.S. Atlantic margin, *Geochem. Geophys. Geosyst.*, *8*, Q12008, doi:10.1029/2007GC001722.

Hühnerbach, V., D. G. Masson, and partners of the COSTA-Project (2004), Landslides in the North Atlantic and its adjacent seas: An analysis of their morphology, setting and behaviour, *Mar. Geol.*, *213*, 343–362, doi:10.1016/j.margeo.2004.10.013.

Hustoft, S., B. Dugan, and J. Mienert (2009), Effects of rapid sedimentation of developing the Nyegga pockmark field: Constraints from hydrological modeling and 3-D seismic data, offshore mid-Norway, *Geochem. Geophys. Geosyst.*, *10*, Q06012, doi:10.1029/2009GC002409.

Kayen, R. E., and H. J. Lee (1991), Pleistocene slope instability of gas hydrate-laden sediment on the Beaufort sea margin, *Mar. Geotechnol.*, *10*(1–2), 125–141, doi:10.1080/10641199109379886.

Keller, G. H. (1982), Organic matter and the geotechnical properties of submarine sediments, *Geo-Mar. Lett.*, *2*, 191–198, doi:10.1007/BF02462762.

Korup, O., J. J. Clague, R. L. Hermanns, K. Hewitt, A. L. Strom, and J. T. Weidinger (2007), Giant landslides, topography, and erosion, *Earth Planet. Sci. Lett.*, *261*(3–4), 578–589, doi:10.1016/j.epsl.2007.07.025.

Kowsmann, R. O., L. C. R. Machado, A. R. Viana, W. Almeida, and M. A. Vicalvi (2002), Controls on mass-wasting in deep water of the Campos Basin, paper presented at Offshore Technology Conference, Houston, Tex., 6-9 May.

Krastel, S., R. B. Wynn, A. Georgiopoulou, J. Geersen, R. Henrich, M. Meyer, and T. Schwenk (2012), Large-scale mass wasting on the Northwest African Continental Margin: Some general Implications for mass wasting on passive continental margins, in *Submarine Mass Movements and Their Consequences, Advances in Natural and Technological Hazards Research*, vol. 31, edited by Y. Yamada et al., pp. 189–199, Springer, Netherlands, doi:10.1007/978-94-007-2162-3_17.

Kvalstad, T. J., L. Andresen, C. F. Forsberg, K. Berg, P. Bryn, and M. Wangen (2005), The Storegga Slide: Evaluation of triggering sources and slide mechanics, *Mar. Pet. Geol.*, *22*, 245–256, doi:10.1016/j.marpetgeo.200410.1019.

Lee, C., T. S. Yun, J. S. Lee, J. J. Bahk, and J. C. Santamarina (2011), Geotechnical characterization of marine sediments in the Ulleung Basin, East Sea, *Eng. Geol.*, *117*, 151–158, doi:10.1016/j.enggeo.2010.10.014.

Lee, H. J. (2009), Timing and occurrence of large submarine landslides on the Atlantic Ocean Margin, *Mar. Geol.*, *264*, 53–64, doi:10.1016/j.margeo.2008.09.009.

Leynaud, D., N. Sultan, and J. Mienert (2007), The role of sedimentation rate and permeability in the slope stability of the formerly glaciated Norwegian continental margin: The Storegga Slide model, *Landslides*, *4*, 297–309, doi:10.1007/s10346-007-0086-z.

Locat, J., and H. J. Lee (2002), Submarine landslides: Advances and challenges, *Can. Geotech. J.*, *39*, 193–212, doi:10.1029/95RG03287.

Long, H., P. Flemings, J. Germaine, and D. Saffer (2011), Consolidation and overpressure near the seafloor in the Ursa Basin, deepwater Gulf of Mexico, *Earth Planet. Sci. Lett.*, *305*(1–2), 11–20, doi:10.1016/j.epsl.2011.02.007.

Masson, D. G., C. B. Harbitz, R. B. Wynn, G. Pedersen, and F. Løvholt (2006), Submarine landslides: Processes, triggers and hazard prediction, *Philos. Trans. R. Soc.*, *364*, 2009–2039, doi:10.1098/rsta.2006.1810.

Masson, D. G., R. B. Wynn, and P. J. Talling (2010), Large landslides on passive continental margins: Processes, hypotheses and outstanding questions, in *Submarine Mass Movements and Their Consequences, Advances in Natural and Technological Hazards Research*, vol. 28, edited by D. C. Mosher et al., pp. 153–165, Springer, Netherlands, doi:10.1007/978-90-481-3071-9-13.

McAdoo, B. G., L. F. Pratson, and D. L. Orange (2000), Submarine landslide geomorphology, US continental slope, *Mar. Geol.*, *169*, 103–136, doi:10.1016/S0025-3227(00)00050-5.

Milliman, J. D., and J. P. M. Syvitski (1992), Geomorphic/tectonic control of sediment discharge to the ocean: The importance of small mountainous rivers, *J. Geol.*, *100*, 525–544.

Mulder, T., J.-P. Tisot, P. Cochonat, and J.-F. Bourillet (1994), Regional assessment of mass failure events in the Baie des Anges, Mediterranean Sea, *Mar. Geol.*, *122*(1–2), 29–45, doi:10.1016/0025-3227(94)90203-8.

Palmer-Julson, A., and F. R. Rack (1992), The relationship between sediment fabric and planktonic microfossil taphonomy: How do plankton skeletons become pelagic ooze?, *PALAIOS*, *7*(2), 167–177.

Pastouret, L., H. Chamley, G. Delibrias, J.-C. Duplessy, and J. Thiede (1979), Late Quaternary climatic changes in Western Tropical Africa deduced from deep-sea sedimentation off Niger Delta, *Oceanol. Acta*, *1*(2), 217–232, doi:10.1594/PANGAEA.707458.

Piper, D. J. W., and A. E. Aksu (1987), The source and origin of the 1929 Grand Banks turbidity current inferred from sediment budgets, *Geo-Mar. Lett.*, *7*(4), 177–182, doi:10.1007/BF02242769.

Powrie, W. (2002), *Soil Mechanics*, 675 pp., Spon, London, U. K.

Premuzic, E. T., C. M. Benkovitz, J. S. Gaffney, and J. J. Walsh (1982), The nature and distribution of organic matter in the surface sediments of world oceans and seas, *Org. Geochem.*, *4*(2), 63–77, doi:10.1016/0146-6380(82)90009-2.

Pusch, R. (1973), Influence of salinity and organic matter on the formation of clay microstructures, in *International Symposium on Soil Structure*, pp. 161–173, Stockholm, Gotenburg, Sweden.

Rack, F., W. Bryant, and A. Julson (1993), Microfabric and physical properties of deep-sea high latitude carbonate oozes, in *Carbonate Microfabrics, Frontiers in Sedimentary Geology*, edited by R. Rezak and D. Lavoie, pp. 129–147, Springer, New York., doi:10.1007/978-1-4684-9421-1_10.

Reece, J. S., P. B. Flemings, B. Dugan, H. Long, and J. T. Germaine (2012), Permeability-porosity relationships of shallow mudstones in the Ursa Basin, northern deepwater Gulf of Mexico, *J. Geophys. Res.*, *117*, B12102, doi:10.1029/2012JB009438.

Richards, A. F., and E. L. Hamilton (1967), *Investigations of Deep-Sea Sediment Cores. III. Consolidation*, Univ. of Ill. Press, Chicago.

Roscoe, K. H., and J. B. Burland (1968), *Engineering Plasticity*, chap. On the generalised stress–strain behaviour of 'wet' clay, pp. 535–609, Cambridge Univ. Press, Cambridge, U. K.

Ruddiman, W., M. Sarnthein, and Expedition 108 Scientists (1988), *Proceedings of the Ocean Drilling Program, Scientific Results*, pp. 1–519, Ocean Drilling Program, College Station, Tex.

Schiffman, R. L., V. Pane, and R. E. Gibson (1984), The theory of one-dimensional consolidation of clays. IV. An overview of nonlinear finite strain sedimentation and consolidation, in *Proceedings of the Symposium on Sedimentation-Consolidation Models: Prediction and Validation*, pp. 1–29, Am. Soc. of Civil Eng., New York.

Schneider, J., P. B. Flemings, B. Dugan, H. Long, and J. T. Germaine (2009), Overpressure and consolidation near the seafloor of Brazos-Trinity Basin IV, northwest deepwater Gulf of Mexico, *J. Geophys. Res.*, *114*, B05102, doi:10.1029/2008JB005922.

Shiwakoti, D. R., H. Tanaka, M. Tanaka, and J. Locat (2002), Influences of diatom microfossils on engineering properties of soils, *J. Jpn. Geotech. Soc. Soils Found.*, *42*(3), 1–17, doi:10.3208/sandf.42.3_1.

Skempton, A. W. (1970), The consolidation of clays by gravitational compaction, *Q. J. Geol. Soc. London*, *125*, 373–411, doi:10.1144/gsjgs.125.1.0373.

Stigall, J., and B. Dugan (2010), Overpressure and earthquake initiated slope failure in the Ursa region, northern Gulf of Mexico, *J. Geophys. Res.*, 115, B04101, doi:10.1029/2009JB006848.

Sultan, N., et al. (2004), Triggering mechanisms of slope instability processes and sediment failures on continental margins: A geotechnical approach, *Mar. Geol.*, *213*(1–4), 291–321, doi:10.1016/j.margeo.2004.10.011.

Tada, R. (1991), *Cycles and Events in Stratigraphy*, chap. Compaction and cementation in siliceous rocks and their possible effect on bedding enhancement, pp. 480–491, Springer, Heidelberg.

Talling, P., M. Clare, M. Urlaub, E. Pope, J. Hunt, and S. Watt (2014), Large submarine landslides on continental slopes: Geohazards, methane release, and climate change, *Oceanography*, *27*(2), 32–45, doi:10.5670/oceanog.2014.38.

Tanaka, H., and J. Locat (1999), A microstructural investigation of Osaka Bay clay: The impact of microfossils on its mechanical behaviour, *Can. Geotech. J.*, *36*(3), 493–508, doi:10.1139/t99-009.

Tappin, D. R., P. Watts, G. M. McMurtry, Y. Lafoy, and T. Matsumoto (2001), The Sissano, Papua New Guinea tsunami of July 1998—Offshore evidence on the source mechanism, *Mar. Geol.*, *175*, 1–23, doi:10.1016/S0025-3227(01)00131-1.

Twichell, D. C., J. D. Chaytor, U. S. ten Brink, and B. Buczkowski (2009), Morphology of late Quaternary submarine landslides along the U.S. Atlantic continental margin, *Mar. Geol.*, *264*, 4–15, doi:10.1016/j.margeo.2009.01.2009.

Urlaub, M., A. Zervos, P. J. Talling, D. G. Masson, and C. I. Clayton (2012), How do 2° slopes fail in areas of slow sedimentation? A sensitivity study on the influence of accumulation rate and permeability on submarine slope stability, in *Submarine Mass Movements and Their Consequences, Advances in Natural and Technological Hazards Research*, vol. 31, edited by Y. Yamada et al., pp. 277–287, Springer, Netherlands, doi:10.1007/978-94-007-2162-3_25.

Valent, P. J., A. G. Altschaeffl, and H. J. Lee (1982), Geotechnical properties of two calcareous oozes, in *Geotechnical Properties, Behavior and Performance of Calcareous Soils*, edited by K. R. Demars and R. C. Chaney, pp. 79–95, Am. Soc. for Testing and Materials, Philadelphia, Pa.

Veyera, G., H. Brandes, and A. Silva (2001), Geotechnical characterization of calcareous sediments from the Dry Tortugas Keys and Marquesas Keys CBBL SRP study sites, Lower Florida Keys, *Geo-Mar. Lett.*, *21*(3), 131–148, doi:10.1007/s003670100075.

Viesca, R. C., and J. R. Rice (2012), Nucleation of slip-weakening rupture instability in landslides by localized increase of pore pressure, *J. Geophys. Res.*, *117*, B03104, doi:10.1029/2011JB008866.

Voight, B., R. J. Janda, and H. Glicken (1985), Nature and mechanics of the Mount St. Helens rockslide-avalanche of 18 May 1980, *Geotechnique*, *33*, 243–273.

Volpi, V., A. Camerlenghi, C.-D. Hillenbrand, M. Rebesco, and R. Ivaldi (2003), Effects of biogenic silica on sediment compaction and slope stability on the Pacific margin of the Antarctic Peninsula, *Basin Res.*, *15*(3), 339–363, doi:10.1046/j.1365-2117.2003.00210.x.

Wangen, M. (2000), Generation of overpressure by cementation of pore space in sedimentary rocks, *Geophys. J. Int.*, *143*(3), 608–620, doi:10.1046/j.1365-246X.2000.00248.x.

Weaver, P. P. E., R. B. Wynn, N. H. Kenyon, and J. Evans (2000), Continental margin sedimentation, with special reference to the north-east Atlantic margin, *Sedimentology*, *47*, 239–256, doi:10.1046/j.1365-3091.2000.0470s1239.

Wetzel, A. (1990), Interrelationships between porosity and other geotechnical properties of slowly deposited, fine-grained marine surface sediments, *Mar. Geol.*, *92*(1–2), 105–113, doi:10.1016/0025-3227(90)90029-J.

Won, J. Y., and P. W. Chang (2007), The causes of apparent overconsolidation in the Namak marine deposit, Korea, *Geotechnique*, *57*, 355–369, doi:10.1680/geot.2007.57.4.355.

Wynn, R. B., D. G. Masson, D. A. V. Stow, and P. P. E. Weaver (2000), The Northwest African slope apron: A modern analogue for deep-water systems with complex seafloor topography, *Mar. Pet. Geol.*, *17*, 253–265, doi:10.1016/S0264-8172(99)00014-8.

Zankl, H. (1969), Structural and textural evidence of early lithification in fine-grained carbonate rocks, *Sedimentology*, *12*(3–4), 241–256, doi:10.1111/j.1365-3091.1969.tb00877.x.